Tracing quark and dark matter signals in neutron stars through inspiral stage gravitational waves

Bin Hong[*] and ZhongZhou Ren[†]

School of Physics Science and Engineering, Tongji University, Shanghai 200092, China
and Key Laboratory of Advanced Micro-Structure Materials, Ministry of Education,
Shanghai 200092, China

The recent detection of gravitational waves from a binary neutron star merger event offers a unparalleled insight into the dense matter. Meanwhile, the existence of quark matter within neutron stars, potentially forming hybrid stars or even strange quark stars, and the possible presence of dark matter mixed within these compact stars remain a matter of debate. To address this, our study explores the inspiral processes of various binary compact star systems, including binary hybrid stars, binary strange quark stars, as well as their corresponding dark matter-mixed counterparts, to decode the signatures imprinted in inspiral gravitational waves. Our analysis reveals that the inspiral process of hybrid stars and strange quark stars exhibit higher gravitational wave frequencies and longer retarded times than that of traditional neutron stars. Mixing dark matter components into these systems further amplifies these signals, increasing the frequency and extending the inspiral duration even more. These findings highlight the critical roles of dark matter and quark matter in determining the features of inspiral gravitational waves, providing vital clues for future observations. Moreover, our study also suggests the use of inspiral gravitational waves can play an effective tool to decipher the signals of quark and dark matter within neutron stars.

I. INTRODUCTION

The nature of matter at extremely high densities is still an unresolved scientific issue [1,2]. Fortunately, neutron stars (NSs), with their unique conditions, serve as a natural laboratory for exploring such states of matter, displaying a variety of phenomena driven by the strong gravitational fields and intense magnetic fields [1–3]. Recent advancements in multimessenger astronomy have propelled forward our understanding of NSs [4–14]. Notable observations include the identification of NSs with masses around twice solar mass ($M_\odot$), Pulsar (PSR) J1614 − 2230 in 2010 [4,5] and PSR J0048 + 0432 in 2013 [6], the groundbreaking observation of a binary NS merger GW170817 event with simultaneous electromagnetic spectrum by the LIGO/Virgo collaboration [7], the discovery of a compact companion with $M = 2.5$–$2.67 M_\odot$ in GW190814 [8], the precise mass and radius measurements from Neutron Star Interior Composition Explorer (NICER) [15] for PSR J0030 + 0451 [9,10] and PSR J0740 + 6620 [11,12], and the identification of the fastest and heaviest NS with $M_{max} = 2.35 \pm 0.17 M_\odot$ for the black widow pulsar PSR J0952 − 0607 [13]. Additionally,

analysis of the supernova remnant HESS J1731-347 revealed a very exotic compact object with an incredibly low mass of $M = 0.77^{+0.20}_{-0.17} M_\odot$ and a very small radius of $R = 10.4^{+0.86}_{-0.78}$ km [14], raising a concern about reconciling such peculiar compact star in traditional NS models.

To reconcile these observational constraints, theoretical advancements have kept pace [16–22]. For instance, the covariant density functional theory proposes that massive NSs, under the dubbed "BigApple" parameter, can be described in nucleon degrees of freedom alone [16], the introducing of hyperon by adjusting the hypernuclear potential well depth [17] or the incorporating of quark degrees of freedom [18] can effectively explain the light companion observed in GW190814 gravitational wave event. Moreover, to reach an agreement on the characteristics of central compact object in HESS J1731-347 [14], incorporating delta meson effects [19], employing a quark-core hybrid model [20], postulating a smaller symmetry energy slope in the baryon model [21], or mixing dark matters (DMs) in NSs [22] could reconcile such object to some extent. Despite these developments have introduced new insights into the equation of states (EoSs) for NSs, a critical consensus on the description of the matter inside NSs has yet to be achieved, with the most heated one being whether the interior of a NS entirely consists of pure nucleon or other degrees of freedom

[*]hongbin@tongji.edu.cn
[†]zren@tongji.edu.cn

such as hyperons [23,24], kaon mesons [25,26], pion mesons [27], quarks [28–33], and even DMs [34]; thus, further in-depth research remains essential.

Since Witten's hypothesis [35–37] that u, d, and s quarks may form the most stable state in nature, and given that the high-density regions inside NSs can provide excellent sites for quarks [38], there has been a surge in research focused on the examination of quarks within NSs [39–43]. This exploration is driven by the hypothesis that the quarks within NSs could manifest in the form of hybrid stars which characterized by nucleon matter enveloped on the surface and quark matter inside or as self-bound strange quark stars that are composed entirely of three quark flavors. Additionally, the potential for NS strong gravitational field to capture DMs has opened new avenues for research, when DMs are extended to the NSs to form the DM-mixed counterparts, it can have a significant impact on the NS properties like mass-radius and asteroseismology frequency [44–47]. Although ongoing debates about the nature of DM, in particular the search and verification of candidates that urgently need input from experiments such as the PandaX-II [48], its existence has long been confirmed by observations, including the cosmic microwave background, the rotation curves of galaxies, and gravitational lensing [49,50]. Introducing quark matter and DM into NSs could significantly affect their properties, but the interactions between them as well as their detection remain underexplored, addressing these challenges is crucial for a deeper understanding internal structure of NSs.

In this paper, within the constraints imposed by observational evidence [4,5,7,9–12], we explore quark and DM components in DM-mixed hybrid stars and DM-mixed strange quark stars. Our goal is attempt to seek possible quark and DM imprints left on binary compact star inspiral gravitational waves. Although the confirmed gravitational wave data on binary NSs merger are as yet scarce, with only the GW170817 event available for extracting effective tidal deformability and its exact range is still subject to disagreements, the use of gravitational wave to decode different compact star types is still an active area. Additionally, multi-messenger observations have refined our understanding of NS structures that eliminate the most unrealistic EoSs, but differentiating between various components, especially the quark matters and DMs within NSs still remain a serious challenge.

The paper is structured as follows: In Sec. II, we outline in detail how to construct reliable microscopic EoSs for the hybrid stars and strange quark stars, as well as their DM-mixed counterparts. In Sec. III, we address the signals from quark and dark matter in tidal deformability, and attempt to explore the imprints of quark and DM in modulating the binary NS inspiral gravitational waves. In Sec. IV, we give a brief summary.

II. MICROSCOPIC MODELS

In this section, we outline theoretical models characterizing hybrid stars, strange quark stars, and their corresponding mixed DM models. For the baryon matter components associated in hybrid stars, we employ the relativistic mean-field theory model [51–57]. For the quark components in hybrid stars and strange quark stars, we consider a density-dependent bag model [58,59]. As for the DM components mixed in above compact stars, we consider relativistic fermion candidate particles [60].

A. Baryon matter model in relativistic mean-field theory

The relativistic mean-field theory (RMFT), serving as a phenomenological nuclear quantum many-body theory, has demonstrated significant advantages in describing nuclear matter, atomic nucleus systems, and NSs [51–57]. In the RMFT, the interaction between nucleons occurs through the exchange of different mesons. A typical representation includes the scalar-isoscalar meson σ, characterizing the medium-range attractive nuclear force; the vector-isoscalar meson ω, describing short-range repulsion; and the vector-isovector mesons ρ and δ, which depict nucleon isospin effects. In this paper, we adopt a simplified version known as the "$\sigma\omega\rho$" meson exchange model, which adequately highlights the features of RMFT and has also been widely employed to describe the NS properties [56,57]. The Lagrangian density in NS system can be expressed in the following form:

$$
\begin{aligned}
L = \sum_{N=n,p} \bar{\psi}_N \Bigg(&\mathrm{i}\partial_\mu\gamma^\mu - m_N + g_\sigma\sigma - g_\omega\omega_\mu\gamma^\mu \\
&- \frac{1}{2}g_\rho\vec{\rho}_\mu\gamma^\mu\vec{\tau} \Bigg)\psi_N + \frac{1}{2}\partial_\mu\sigma\partial^\mu\sigma - \frac{1}{2}m_\sigma^2\sigma^2 - \frac{1}{4}c(g_\sigma\sigma)^4 \\
&- \frac{1}{3}bm_N(g_\sigma\sigma)^3 + \Lambda_\omega(g_\rho^2\rho^\mu\rho_\mu)(g_\omega^2\omega^\mu\omega_\mu) \\
&- \frac{1}{4}(\partial_\mu\vec{\rho}_v - \partial_\nu\vec{\rho}_\mu)(\partial^\mu\vec{\rho}^\nu - \partial^\nu\vec{\rho}^\mu) + \frac{1}{2}m_\rho^2\vec{\rho}_\mu\vec{\rho}^\mu \\
&- \frac{1}{4}(\partial_\mu\omega_v - \partial_\nu\omega_\mu)(\partial^\mu\omega^\nu - \partial^\nu\omega^\mu) + \frac{1}{2}m_\omega^2\omega_\mu\omega^\mu \\
&+ \sum_{l=e,\mu}\bar{\psi}_l(i\partial_\mu\gamma^\mu - m_l)\psi_l,
\end{aligned}
\tag{1}
$$

where N and l stand for nucleons (n, p) and leptons (e, μ) in the NS beta-equilibrium system, and m_i (where $i = N, l, \sigma, \omega, \rho$) stands for the mass of nucleons, leptons, and mesons. The corresponding energy density and pressure of nucleon matter (NM) can be expressed as follows:

$$\varepsilon_{\mathrm{NM}} = \sum_N g_\omega \omega_0 \frac{k_N^3}{3\pi^2} + \frac{1}{\pi^2} \int_0^{k_N} k^2 \sqrt{k^2 + (m_N^*)^2} dk$$

$$+ \sum_l \frac{1}{\pi^2} \int_0^{k_l} k^2 \sqrt{k^2 + m_l^2} dk + \frac{1}{2} m_\sigma^2 \sigma_0^2 - \frac{1}{2} m_\omega^2 \omega_0^2$$

$$- \frac{1}{2} m_\rho^2 \rho_0^2 - \Lambda_\omega (g_\rho \rho_0)^2 (g_\omega \omega_0)^2 + \frac{1}{3} g_2 \sigma_0^3 + \frac{1}{4} g_3 \sigma_0^4,$$

$$p_{\mathrm{NM}} = -\frac{1}{2} m_\sigma^2 \sigma_0^2 + \frac{1}{2} m_\omega^2 \omega_0^2 + \frac{1}{2} m_\rho^2 \rho_0^2 - \frac{1}{3} g_2 \sigma_0^3 - \frac{1}{4} g_3 \sigma_0^4$$

$$+ \frac{1}{3} \sum_l \frac{1}{\pi^2} \int_0^{k_l} \frac{k^4}{\sqrt{k^2 + m_l^2}} dk$$

$$+ \frac{1}{3} \sum_N \frac{1}{\pi^2} \int_0^{k_N} \frac{k^4}{\sqrt{k^2 + (m_N^*)^2}} dk$$

$$+ \Lambda_\omega (g_\rho \rho_0)^2 (g_\omega \omega_0)^2, \tag{2}$$

with the coupling parameters of $g_\sigma, g_\omega, g_\rho, g_2, g_3, \Lambda_\omega$ being typically determined by fitting the empirical saturation properties (saturation density n_0, incompressibility coefficient K, binding energy E/A, effective mass m^*, symmetry energy E_{sym}, and its slope L). As we know, there are many excellent parameter sets like FSUGold [61], NL3 [62], BigApple [16], IOPB-I [63], FSUGarnet [64], DOPS series [65], and OMEG series [66], which are commonly utilized in RMFT by incorporating new interactions, making the coupling parameters highly model dependent. In this study, as we primarily focus on DM and quark components, for the nucleons, our attention is exclusively focused on assessing whether the coupling parameter can yield NSs consistent with current astronomical observations. To simplify the analysis, we adopt an approach similar to the one introduced in [67], where the nucleon coupling parameters exhibit a well-defined arithmetic relationship with the nuclear saturation properties. For a detailed derivation, please refer to references [67–69]. The nuclear saturation properties we use here are $n_0 = 0.16$ fm^{-3} [70], $K = 230$ MeV [71], $E/A = -16$ MeV [67], $m^* = 0.70$ [67], $E_{\mathrm{sym}} = 32$ MeV [72], $L = 70$ MeV [3], and the corresponding coupling parameters give $g_\sigma = 9.588$, $g_\omega = 10.355$, $g_\rho = 8.941$, $g_2 = 20.807$ fm^{-1}, $g_3 = -45.989$, $\Lambda_\omega = 0.026$. Furthermore, in the established NS computational framework, for the outer crust component characterized by densities in the range of 6.3×10^{-12} fm$^{-3} \leq n \leq 2.46 \times 10^{-4}$ fm^{-3}, we adopt the Baym-Pethick-Sutherland EoS [73], and for the inner crust region, where densities span from 2.46×10^{-4} fm$^{-3} \leq n \leq n_t$, the polytropic parametrized EoS is applied [74,75].

B. Quark model in hybrid stars and strange quark stars

Growing evidence now suggests that quark matter should be present in the interiors of compact stars, such as NSs [38]. This implies that at sufficiently high densities, matter may undergo a transition from quark-confined baryon states to deconfined quark matter states. According to the Bodmer-Terazawa-Witten hypothesis [35–37], the strange matter consisting of almost equal amounts of u, s, d quark may be absolutely stable in nature; i.e., its energy per baryon is less than the conventional iron binding energy, and, if this hypothesis holds, all baryon matter would transform into quark matter, leading to the conversion of NSs into strange quark stars. In our modeling of a strange quark star, we consider massless u, d quarks and finite-mass singlet s quark with $m_s = 200$ MeV [29] and allow for transitions between quarks and leptons via weak interactions. The thermodynamic potential of the system as the chemical potential of the components can be written in the form of [28,29]

$$\Omega_u = -\frac{\mu_u^4}{4\pi^2} \left[1 - \frac{2\alpha_c}{\pi} \right], \tag{3}$$

$$\Omega_d = -\frac{\mu_d^4}{4\pi^2} \left[1 - \frac{2\alpha_c}{\pi} \right], \tag{4}$$

$$\Omega_s = -\frac{1}{4\pi^2} \left\{ \mu_s (\mu_s^2 - m_s^2)^{1/2} \left(\mu_s^2 - \frac{5}{2} m_s^2 \right) + \frac{3}{2} m_s^4 \right.$$

$$\times \ln \frac{\mu_s + (\mu_s^2 - m_s^2)^{1/2}}{m_s} - \frac{2\alpha_c}{\pi} \left[3 \left[\mu_s (\mu_s^2 - m_s^2)^{1/2} \right.\right.$$

$$- m_s^2 \ln \frac{\mu_s + (\mu_s^2 - m_s^2)^{1/2}}{\mu_s} \right]^2 - 2(\mu_s^2 - m_s^2)^2$$

$$+ 3 m_s^4 \ln^2 \frac{m_s}{\mu_s} + 6 \ln \frac{\varrho}{\mu_s} \left[\mu_s m_s^2 (\mu_s^2 - m_s^2)^{1/2} \right.$$

$$\left.\left.\left. - m_s^4 \ln \frac{\mu_s + (\mu_s^2 - m_s^2)^{1/2}}{m_s} \right] \right] \right\}, \tag{5}$$

where μ_e and $\mu_{u,d,s}$ represent the chemical potentials of electron and quarks. The renormalization point of the strange quark mass, designated by the parameter ϱ, has a value of $\varrho = M_N c^2/3 = 313$ MeV [29]. The chemical potential equilibrium condition written as

$$\mu_u = (\mu_n - 2\mu_e)/3, \tag{6}$$

$$\mu_d = \mu_u + \mu_e = (\mu_n + \mu_e)/3, \tag{7}$$

$$\mu_s = \mu_d, \tag{8}$$

with μ_n being neutron chemical potential. The charge neutrality condition are

$$\frac{2}{3} n_u(\mu_u) = \frac{1}{3} [n_d(\mu_d) + n_s(\mu_s)] + n_e(\mu_e). \tag{9}$$

Taking into account the vacuum bag model constant B, the pressure and energy density of quark matter (QM) can be

expressed as follows

$$P_{QM} = -\sum_{i=u,d,s} \Omega_i(\mu) - B, \qquad (10)$$

$$\varepsilon_{QM} = \sum_{i=u,d,s} (\Omega_i + \mu_i n_i) + B. \qquad (11)$$

It is well known that the MIT bag model, developed by physicists at the Massachusetts Institute of Technology (MIT), is characterized by the bag constant B, which is actually the difference in energy density between the perturbed vacuum and the real vacuum, and it is usually seen as a free parameter. In this paper, we use the density-dependent bag model, which considers the bag constant to exhibit a Gaussian-type distribution with density [58,59]

$$B(\rho) = B_{as} + (B_0 - B_{as}) \exp\left[-\beta(\rho/\rho_0)^2\right], \qquad (12)$$

where the parameter β controls the variation of the bag constant with density, reaching a finite value B_0 at $\rho = 0$ and approximating B_{as} at asymptotic densities. In this study, following the suggestions of [58,59,76], we have chosen to model the strange quark star using parameters $B_0 = 400$ MeV/fm^3 and $\beta = 0.17$, while leaving B_{as} as a variable to characterize the quark matter impact, with employing values of 50 and 80 MeV for following investigation.

To model a hybrid star, we use the RMFT to describe the nucleon matter and above-mentioned density-dependent bag model for quark matter. As for the transition region from nucleon component to quark component, the Gibbs construction (GC) [77] are used, for a detailed sketch of GC configuration we recommend Refs. [78,79]. The GC suggests that there is a coexistence mixed phase (CMP) in the transition from baryons to quarks, where the pressure and the chemical potential of nucleons and electrons are continuous, in the form of

$$P_{NM}(\mu_{n,NM}, \mu_{e,NM}) = P_{QM}(\mu_{n,QM}, \mu_{e,QM}) = P_{CMP},$$

$$\mu_{n,NM} = \mu_{n,QM}, \qquad \mu_{e,NM} = \mu_{e,QM}. \qquad (13)$$

The region where quarks and baryons coexist satisfies global charge conservation

$$\chi \rho_{QM} + (1-\chi)\rho_{NM} = 0, \qquad (14)$$

where χ is the fraction of quarks in the coexistence region whose value changes continuously from the baryon term $\chi = 0$ to the quark phase $\chi = 1$. Therefore, the energy density and baryon density of the coexistence mixed phase are expressed as

$$\varepsilon_{CMP} = \chi \varepsilon_{QM} + (1-\chi)\varepsilon_{NM}, \qquad (15)$$

$$\rho_{CMP} = \chi \rho_{QM} + (1-\chi)\rho_{NM}. \qquad (16)$$

C. Dark matter model

In investigation of the DM component mixed in hybrid stars and strange quark stars, we assume the DMs are asymmetric fermi particles [60], with their self-interactions being mediated via a ϕ mediator, characterized by a repulsive Yukawa potential:

$$V = \frac{\alpha_\chi}{r} \exp\left(-m_\phi r\right), \qquad (17)$$

where α_χ signifies the fine-structure constant of DM coupling to dark mediator and we adopt a value of 10^{-3} from [60]. m_ϕ is the mediator mass and generally accepted to be below $50 \sim 60$ GeV [80,81] and theory-based studies primarily focus on 10 GeV [60,82]. In this study, according to the previous work [22], we select m_ϕ serves the variable to describe DM effect, with chosen values of 15 and 20 MeV. The energy density of DM can be expressed as

$$\varepsilon_{DM} = \varepsilon_{kin} + \varepsilon_Y, \qquad (18)$$

with ε_{kin} and ε_Y representing the kinetic energy and Yukawa potential energy density, respectively. The system pressure, from a thermodynamic perspective, is expressed as

$$p_{DM} = n\frac{\partial \varepsilon_{DM}}{\partial n} - \varepsilon_{DM}, \qquad (19)$$

with n being the DM number density. The expressions for kinetic energy density, pressure, and number density of DM are as follows:

$$\varepsilon_{kin} = \frac{g_s}{(2\pi)^3}\int_0^{p_F} E(p)4\pi p^2 dp = \frac{g_s}{2}m_\chi^4\xi(x), \qquad (20)$$

$$p_{kin} = \frac{1}{3}\frac{g_s}{(2\pi)^3}\int_0^{p_F} \frac{p^2}{E(p)}4\pi p^2 dp = \frac{g_s}{2}m_\chi^4\psi(x), \qquad (21)$$

$$n = \frac{g_s}{(2\pi)^3}\int_0^{p_F} 4\pi p^2 dp = \frac{g_s m_\chi^3}{6\pi^2}x^3, \qquad (22)$$

where the relativistic energy dispersion relation is $E = \sqrt{p^2 + m_\chi^2}$, $m_\chi = 2$ GeV is the DM mass and g_s denotes its spin. The terms $\xi(x)$ and $\psi(x)$ are defined as [83]

$$\xi(x) = \frac{1}{8\pi^2}\left\{x\sqrt{1+x^2}(1+2x^2) - \ln\left[x+\sqrt{1+x^2}\right]\right\},$$

$$\psi(x) = \frac{1}{8\pi^2}\left\{x\sqrt{1+x^2}(2x^2/3-1) + \ln\left[x+\sqrt{1+x^2}\right]\right\},$$

with x being defined in terms of the Fermi momentum p_F/m_χ. To precisely measure the total Yukawa potential

energy, it is theoretically required to sum over all DM particles and then approximate the integral over their volume elements. This leads to the expression as

$$\varepsilon_Y = \frac{2\pi\alpha_\chi n^2}{m_\phi^2} = \frac{\alpha_\chi g_s^2}{18\pi^3} \frac{m_\chi^6}{m_\phi^2} x^6. \tag{23}$$

Accordingly, the total energy density and pressure of the DM component can be expressed as [82]

$$\varepsilon_{DM} = \frac{g_s}{2} m_\chi^4 \xi(x) + \frac{\alpha_\chi g_s^2}{18\pi^3} \frac{m_\chi^6}{m_\phi^2} x^6, \tag{24}$$

$$p_{DM} = \frac{g_s}{2} m_\chi^4 \psi(x) + \frac{\alpha_\chi g_s^2}{18\pi^3} \frac{m_\chi^6}{m_\phi^2} x^6. \tag{25}$$

As part of the standard procedure for solving hybrid stars and strange stars, as well as their corresponding mixed dark matter models, the Tolman-Oppenheimer-Volkoff (TOV) equation requires the system EoSs as input parameters. Given that only gravitational interactions exist between the DM particles and the standard particles, the traditional TOV equation will be modified to a two-fluid form (see Refs. [84,85] for a detailed derivation)

$$\frac{dp_i}{dr} = -\frac{(p_i + \epsilon_i)(M + 4\pi r^3 p)}{r(r - 2M)},$$
$$\frac{dp_D}{dr} = -\frac{(p_D + \epsilon_D)(M + 4\pi r^3 p)}{r(r - 2M)},$$
$$dM_i = 4\pi r^2 \epsilon_i dr, \qquad dM_D = 4\pi r^2 \epsilon_D dr, \tag{26}$$

where label i represents hybrid stars and strange quark stars, and label D represents DM component. $p = p_i + p_D$ represents the total pressure at the radius r, and $M = M_i + M_D$ denotes the sum of individual component mass. Given that the DM radius is generally not directly observable, the star radius is usually adopted from the traditional matter component i. The proportion of DM within the compact stars is represented as $f_{DM} = M_D/(M_i + M_D)$, we adopt $f_{DM} = 5\%$ for our analysis in this work. After considering the charge neutrality and chemical potential equilibrium conditions, the mass-radius relationship for the DM-mixed hybrid star and DM-mixed strange quark star systems will be determined. In addition, a relevant stability analysis should be conducted for the two-fluid model. Typically, the stability of stellar structures is discussed by solving the Sturm-Liouville problem to consider small radial perturbations in the equilibrium configuration, with the solutions determined by frequency eigenvalues. For a single fluid, when the first eigenvalue frequency satisfies $\omega^2 \geq 0$, the condition is stable, while a value less than zero leads to an unstable solution [86]. For the two-fluid model, the radial oscillation perturbation equations for ordinary

matter and DM become more complicated. For analysis on the two-fluid stability, we recommend Refs. [86–88] for a review. The following discussion in this paper is also based on the aforementioned stability conditions, and a comprehensive two-fluid stability analysis is expected to be carried out in our future work.

III. NUMERICAL RESULTS AND DISCUSSIONS

A. Mass-radius relationships

The most critical criterion for evaluating theoretical models is whether their predicted mass-radius relationships are consistent with current astronomical observations. In Fig. 1, we present the mass-radius relationships for all considered models, with a special emphasis on the traditional NS scenario with a black curve for comparative purposes. The light-shaded areas show current astronomical observational constraints, including data from NICER observations of PSR J0740 + 6620 and PSR J0030 + 0451 [9–12], the gravitational wave event GW170817 [7], and recent findings from the supernova remnant HESS J1731-347 [14]. The hybrid stars shown in Fig. 1(a), highlighted by red lines, with the dashed and solid lines corresponding to the density-dependent bag model parameter $B_{as} = 50$ MeV and $B_{as} = 80$ MeV, respectively, exhibit softer EoSs than traditional NS when the quark matter starts to appear. In contrast, the absorption of DM to form DM-mixed hybrid stars will result in a further EoS softening, as shown by the dark-blue and green lines for mediator masses of $m_\phi = 20$ MeV and $m_\phi = 15$ MeV, respectively. For example, a typical $1.4M_\odot$ hybrid star with $B_{as} = 50$ MeV has a radius of about 12 km, while decreases to around 11 km when mixed with DM for $m_\phi = 20$ MeV and approximately 10 km for $m_\phi = 15$ MeV. Moreover, all the aforementioned DM-mixed hybrid stars fall in the shaded orange region, which marks the observational constraints from supernova remnant HESS J1731-347, containing an exotic compact object with a mass of about $0.77M_\odot$ and a radius of approximately 10.4 km. This outcome is particularly noteworthy, as the fact that the DM-mixed model employed in our analysis potentially offers a credible explanation for the existence of this peculiar compact object.

The strange quark stars and their DM-mixed counterparts are shown in Fig. 1(b). As highlighted by numerous studies [28–33], the strange quark stars yield smaller radii in low-mass region, giving a completely different mass-radius relation from traditional NSs and hybrid stars. When DM is mixed, the EoSs is also further softened, resulting in smaller masses and radii, as shown by the blue and pink lines. Additionally, from the perspective of satisfying the constraints imposed by HESS J1713-347, our findings suggest that beyond the established quark star model, which has been confirmed as a viable explanation [89],
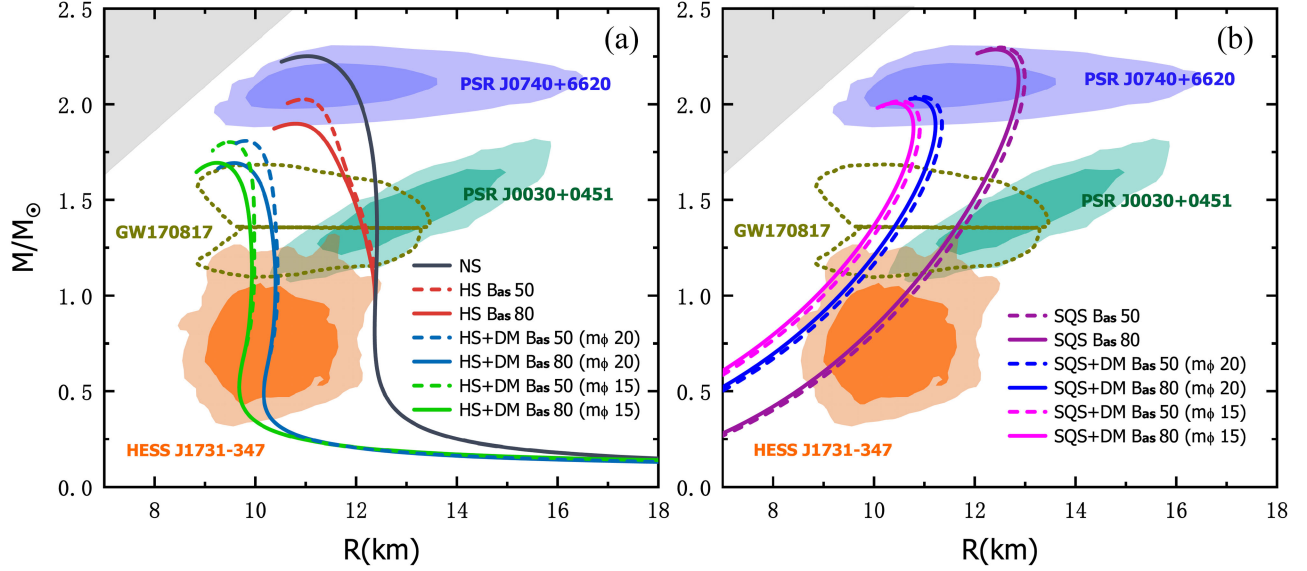
FIG. 1. (a) Mass-radius relationship for the hybrid stars (HS) and its corresponding DM-mixed hybrid stars (HS + DM), in which solid black line marks a NS composed of pure nucleons under RMFT. The red dashed and solid lines, respectively, depict hybrid stars with different quark model parameters B_{as}, while the dark-blue dashed line and solid line represent their corresponding DM-mixed hybrid stars. To compare various DM parameters m_ϕ, we examine the scenario where the DM-mixed hybrid star has a mass of $m_\phi = 15$ MeV, depicted by dashed and solid green lines. The shaded areas suggest the constraints from the PSR J0740 + 6620, PSR J0030 + 0451, and HESS J1731-347. The enclosed dotted contour indicates the observation imposed by GW170817 event. (b) Mass-radius relationship for the strange quark star (SQS) and corresponding DM-mixed model (SQS + DM). The dark-purple dashed and solid lines represent strange quark stars with different B_{as}, while the blue dashed and solid lines depict their corresponding DM-mixed strange quark stars. As a comparison, the solid and dashed pink lines represent DM-mixed strange quark stars with $m_\phi = 15$ MeV.

the DM-mixed quark star models also emerge as a possible scenario.

It should be noted that in solving the two-fluid model, a stability analysis of the stellar is necessary. As pointed out in [87,88,90,91], the stability solution corresponding to the central pressure (or central energy density) of the two-fluid components will form a stable region, rather than just a single curve like in the case of a single-fluid. From Fig. 1(a), we can see that when discussing two-fluid DM-mixed hybrid stars, the regions corresponding to the solid green line and dark-blue line indicate different EoSs, i.e., different central energy densities and central pressures, unlike the single-fluid black solid line where different EoSs fall on a single curve. The same conclusion is true for DM-mixed strange quark stars shown in the Fig. 1(b).

Furthermore, some studies [87,90,91] indicate that near the stability curve, the value of the DM central pressure is generally around the order of 10^3 MeV/fm^3, with values below this threshold indicating a stable region. In our model, whether it is a DM-mixed hybrid star or a DM-mixed strange quark star, the central pressure is far below this value, as will be seen in the lower panels in Figs. 2(b) and 3(b). Therefore, in this regard, the two-fluid models we have chosen satisfies the two-fluid stability feature. More importantly, recent studies have shown that selecting low-mass DM [92,93], as adopted in this work, also more easily meets the stability conditions.

Currently, the capture mechanism of DM in compact stars is still unclear, and the radius of DM distribution, denoted as R_D, often differs from the stellar radius R_i. When R_D is larger than R_i, a DM halo structure is formed, while the opposite scenario results in a DM core. In this study, we fix the DM proportion at 5%, and in order to understand the DM distribution in hybrid stars and strange quark stars in the current model, we also analyze the case with a 50% proportion for comparison with the B_{as} fixed to be 50 MeV. We discuss the DM distribution in typical $1.4M_\odot$ DM-mixed hybrid stars (see Fig. 2) and DM-mixed strange quark stars (see Fig. 3). In Fig. 2, the central pressure of hybrid star is represented by the solid line, while the DM central pressure is represented by the dashed line. Notably, with DM proportion of 50%, R_i surpasses R_D, and a DM core forms. As the DM proportion decreases to 5%, R_i gradually increases, and it can be anticipated that with a further decrease in DM proportion, R_D will exceed R_i, facilitating the formation of a DM halo. Similar conclusions apply to strange quark stars, as illustrated in Fig. 3.

Nevertheless, the model parameters we have employed above could effectively characterize the current observational constraints and both give the DM core structure. Next, we will explore the binary inspiral gravitational waves under these parameter sets.
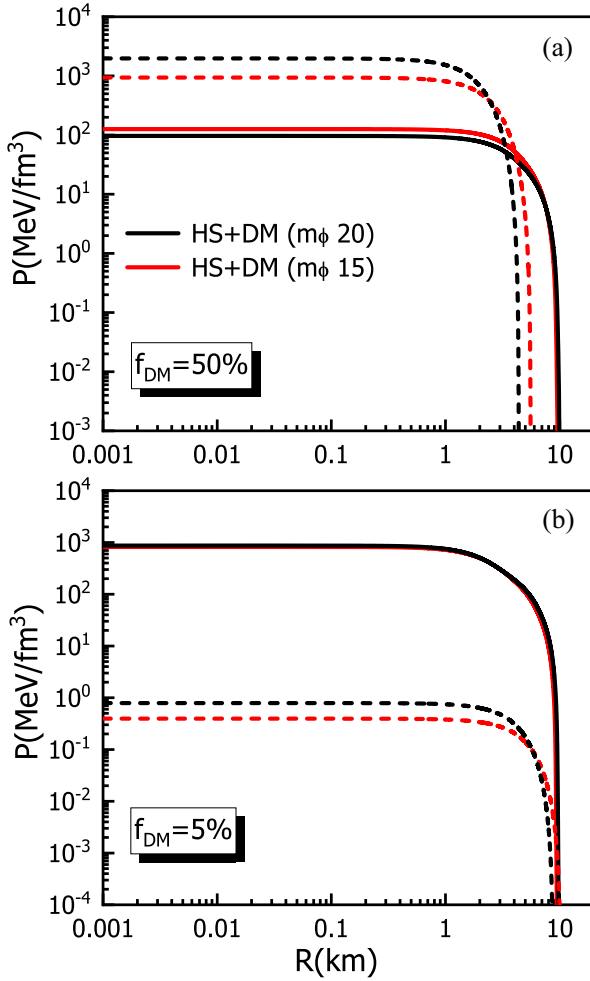
FIG. 2. With DM fraction of (a) 50% and (b) 5%, the central pressure as a function of radius within a $1.4M_\odot$ DM-mixed hybrid star (HS + DM) for different mediator masses of 15 MeV (red color) and 20 MeV (black color). The solid line and dashed line represent HS component and DM component, respectively.

FIG. 3. With DM fraction of (a) 50% and (b) 5%, the central pressure as a function of radius within a $1.4M_\odot$ DM-mixed strange quark star (SQS + DM) with different mediator masses of 15 MeV (red color) and 20 MeV (black color). The solid line and dashed line represent SQS component and DM component.

B. Tidal deformability and binary star inspiral gravitational wave

1. Tidal deformability

Tidal deformability, a dynamical property of stars, serves as a robust indicator of identifying the matter inside compact stars [94–96]. During the binary inspiral process, each compact star will undergo a distortion due to the strong tidal field exerted by its companion. Such distortion is quantitatively characterized by the tidal deformability parameter λ, defined as the ratio between the induced quadrupole moment Q_{ij} and the static external tidal field E_{ij} [94,97]:

$$\lambda = -\frac{Q_{ij}}{E_{ij}}. \tag{27}$$

This quantity is highly dependent on stellar internal components, which offers an unparalleled advantage in constraining the nuclear matter EoSs, and more importantly, could introduce notable tidal-related corrections to the gravitational wave radiation during the inspiral process [98]. Its dimensionless form can usually be expressed in terms of the tidal love factor k_2 as $\Lambda = 2k_2/(3C^5)$, where C is the compact parameter (M/R) and k_2 can be figured out in the following formula [95,96,99,100]:

$$
\begin{aligned}
k_2 = &\frac{8C^5}{5}(1-2C)^2[2+2C(y_R-1)-y_R]\\
&\times \{2C(6-3y_R+3C(5y_R-8))\\
&+4C^3[13-11y_R+C(3y_R-2)+2C^2(1+y_R)]\\
&+3(1-2C)^2[2-y_R+2C(y_R-1)]\log(1-2C)\}^{-1},
\end{aligned}
\tag{28}
$$

with $y_R \equiv y(R)$ satisfying the following first order differential equation

$$r\frac{dy(r)}{dr} + y(r)^2 + y(r)F(r) + r^2Q(r) = 0. \quad (29)$$

For the phase transition from nucleons to quark matter in hybrid stars, the y_R across the transition will be revised as [101,102]

$$y(r_{tr}^+) - y(r_{tr}^-) = -\frac{4\pi r_{tr}^3 \triangle \varepsilon}{M(r_{tr}) + 4\pi r_{tr}^3 P(r_{tr})}, \quad (30)$$

with r_{tr} being the position where nucleon-quark first order phase transition appears. The term $\triangle \varepsilon = \varepsilon(r_{tr}^+) - \varepsilon(r_{tr}^-)$ marks the energy density discontinuity at $r_{tr}^{\pm} = r_{tr} \pm \delta r$, with δr being an infinitesimal shift around phase transition site. For the analysis of strange quark stars, the condition y_R requires adjustment to account for the presence of a finite energy density discontinuity at the stellar surface, which is imposed by the following form [99,103,104]:

$$y_R \rightarrow y_R - \frac{4\pi R^3 \triangle \varepsilon}{M(R) + 4\pi R^3 P(R)}. \quad (31)$$

For the DM-mixed models, it is essential to adopt the two-fluid version of $F(r)$ and $Q(r)$, which also needs to combine the two-fluid TOV equations [Eq. (26)] for numerical solution. We adopt the revised formula of $F(r)$ and $Q(r)$ from the Ref. [105], wherein a in-depth discussion and derivation for this technique can be found.

Figures 4 and 5 depict the tidal deformability and the dimensionless tidal deformability as a function of mass, respectively. The differences between models become more pronounced above $1.4M_\odot$, where quark matter begins to emerge. Given the absence of tidal deformability observations for the compact star similar to the peculiar one in HESS J1731-347, we have illustrated HESS J1731-347 observational constraints shown by the light-shaded area in the figures, wherein the dashed line indicates the maximum credible value. Table I also lists the detailed numerical results of tidal deformability and radius for this compact star under different models. As Fig. 1(a) shows, the values provided by the traditional NS and hybrid star model deviates from the constraint from the HESS J1731-347, thus are considered as failure models in our analysis, as a conclusion also in line with recent studies [14,20,22]. The DM-mixed models show notable differences for HESS J1731-347, with the DM-mixed hybrid stars presenting values ranging from 0.561 to 0.799, approximately five times the values given by DM-mixed strange quark stars, which lie between 0.093 and 0.177. These differentiated results will amplify the tidal-related corrections and consequently be reflected in the emitted gravitational waves
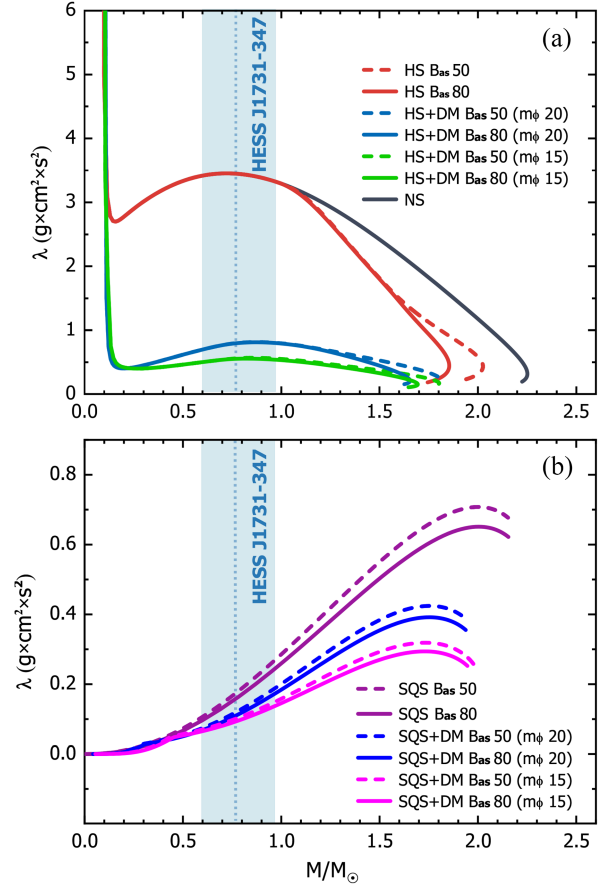
FIG. 4. (a) Tidal deformability as a function of mass for different hybrid stars and their corresponding DM-mixed hybrid stars. The different color curves correspond to respective scenarios in Fig. 1. The vertical shaded region marks the mass range of a recently observed exotic compact star HESS J1731-347, with the dashed line representing its maximum credible value. (b) Tidal deformability for different strange quark stars and their corresponding DM-mixed strange quark stars.

during the binary star inspiral process as discussed in the following subsection.

To facilitate comparison with the GW170817 event, Fig. 5 illustrates the observable dimensionless tidal deformability as a function of mass, wherein all models fall within the constraint marked by the vertical solid black line. Among these, in comparison to the traditional NS, as depicted by the black curve, the presence of quark matter within hybrid stars and strange quark stars exhibits smaller dimensionless tidal deformabilities. Furthermore, the incorporation of DM to form DM-mixed counterparts leads to an additional reduction in tidal deformability. This reduction implies that the quark matter and DM components result in compact stars being less susceptible to distortion in their companion tidal fields, a phenomenon that is even more noticeable in the lower mass region for strange quark stars and their DM-mixed counterparts. If future observations of smaller dimensionless tidal deformability be identified,
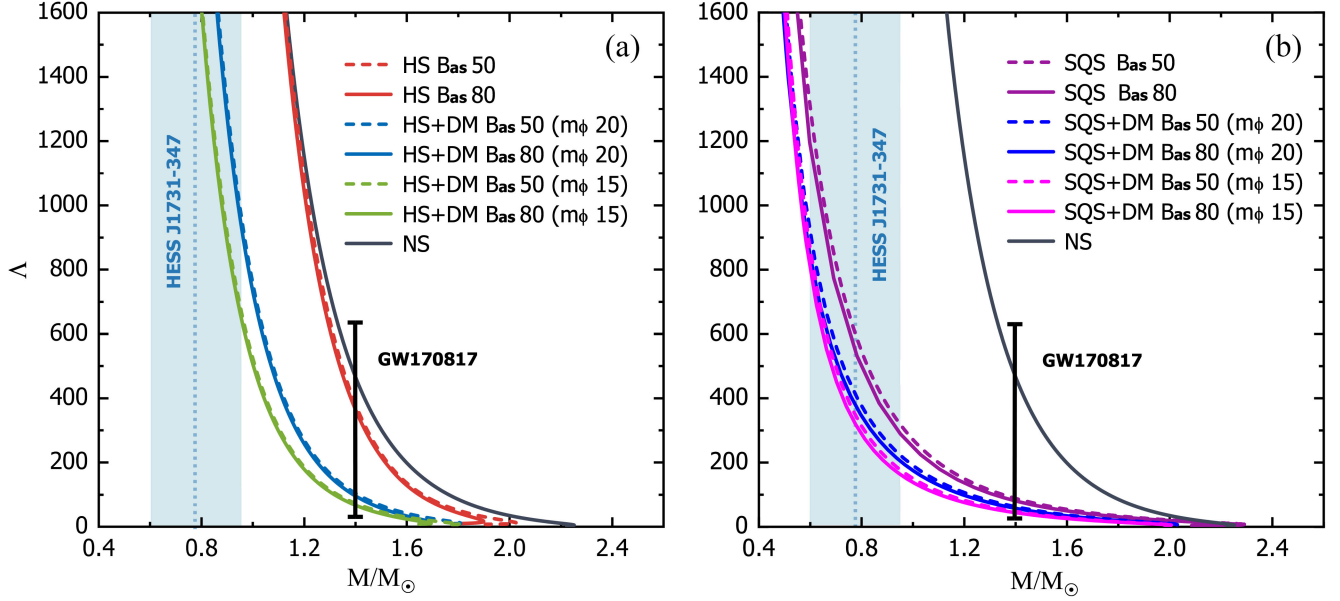
FIG. 5.   (a) Dimensionless tidal deformability as a function of mass for different hybrid stars and corresponding DM-mixed hybrid stars, in which vertical solid black line marks the tidal deformability range extracted from GW170817 event and vertical shaded region marks the mass range of a recently observed peccular compact star in HESS J1731-347. (b) Dimensionless tidal deformability for different strange quark stars and their corresponding DM-mixed strange quark stars.

then it could provide empirical support for the hypothesis of quark matter and DM within NSs.

2. Binary star inspiral phase in quasicircular orbits

In the current endeavor to hunt possible cue of quark matter and DM component within NS, gravitational waves emitted from binary star system have emerged as an

TABLE I.   Predicted values of radius and tidal deformability for the compact object similar to the peculiar one in supernova remnant HESS J1731-347 [14] across various models: Traditional NS, HS, HS + DM, SQS, and SQS + DM. The ✗ implicates the model that are considered unsuccessful for meeting the constraint set by HESS J1731-347.

Case	R (km)	λ (g $\times$ cm^2 $\times$ s^2)
Traditional NS	✗	✗
HS (B$_{as}$ 50)	✗	✗
HS (B$_{as}$ 80)	✗	✗
HS + DM (B$_{as}$ 50 m$_\phi$ 20)	10.38	0.799
HS + DM (B$_{as}$ 80 m$_\phi$ 20)	10.35	0.799
HS + DM (B$_{as}$ 50 m$_\phi$ 15)	9.85	0.561
HS + DM (B$_{as}$ 80 m$_\phi$ 15)	9.85	0.561
SQS (B$_{as}$ 50)	9.09	0.177
SQS (B$_{as}$ 80)	9.74	0.163
SQS + DM (B$_{as}$ 50 m$_\phi$ 20)	8.52	0.128
SQS + DM (B$_{as}$ 80 m$_\phi$ 20)	8.40	0.115
SQS + DM (B$_{as}$ 50 m$_\phi$ 15)	7.89	0.093
SQS + DM (B$_{as}$ 80 m$_\phi$ 15)	7.89	0.093

indispensable tool [106]. The traditional approach interpret the differences in various EoSs have been analyzed from the perspective of stellar bulk properties such as mass radius, gravitational redshift, and moment of inertia. However, the increasing number of observations from binary NSs and NS-black hole merger events has revealed that gravitational wave signals during the inspiral process also carry significant information and has been tirelessly unraveled the uncertainties surrounding the NS internal structures [107,108]. Our subsequent analysis aims to explore the roles of quark matter and DM in shaping the inspiral gravitational wave process. For the sake of clarity, our discussion of the quark model will focus on the scenario where $B_{as} = 50$ MeV. It should be noted that a similar conclusion can be drawn for the case where $B_{as} = 80$ MeV.

The process of binary star coalescence naturally unfolds in three stages [106]: inspiral, merger, and ringdown. Among these, the inspiral phase can be effectively modeled through the post-Newtonian (PN) approximation [109–112]. This approximation, as an expansion of general relativity suitable for scenarios of low velocity and weak gravitational field, has been rigorously tested for its precision [113,114]. The PN approximation treats the binary star system as a quasi-periodic orbit, facilitating precise simulations through high-order corrections in the equations of motion, i.e., expressed as a power series expansion in terms of $\epsilon \sim (v/c)^2 \sim (GM/rc^2)$, with terms of order $(v/c)^n$ corresponding to the $\frac{n}{2}$PN expansion [109,110]. In this study, we employ the Taylor-T4 expanded PN framework [110], a theoretically well-suited method for analyzing gravitational

wave emission during the inspiral phase. A more detailed derivation of this theory can be found in [109,110,115,116].

In the context of gravitational radiation within quasi-circular orbits, the energy luminosity $\mathcal{L}$ is expected to equilibrate with the orbital energy E, as described by

$$\mathcal{L} = -\frac{dE}{dt} = -\frac{dE/dx}{dt/dx}, \qquad (32)$$

where x is a gauge-independent PN parameter, defined by $x = (M_{tot}\frac{d\Phi}{dt})^{2/3} = (M_{tot}\Omega)^{2/3}$. Here, M_{tot} stands for system total mass, Φ for the orbital phase, and Ω for the orbital angular velocity. For a binary star system in quasicircular orbit with $M_{tot} = M_1 + M_2$ and angular velocity Ω, the energy at the 3.5PN order approximates to [109,115,116]

$$E = -\frac{M_{tot}\eta x}{2}\left\{1 + \left(-\frac{3}{4} - \frac{\eta}{12}\right)x + \left(-\frac{27}{8} + \frac{19\eta}{8}\right.\right.$$
$$\left. - \frac{\eta^2}{24}\right)x^2 + \left[-\frac{675}{64} + \left(\frac{34445}{576} - \frac{205\pi^2}{96}\right)\eta\right.$$
$$\left.\left. - \frac{155\eta^2}{96} - \frac{35\eta^3}{5184}\right]x^3\right\}, \qquad (33)$$

with $\eta = m_1 m_2/M_{tot}^2$ denoting the symmetric mass ratio. The 3.5PN order approximation further allows the expression of luminosity $\mathcal{L}$ as [110,115,115,117]

$$\mathcal{L} = \frac{32\eta^2 x^5}{5}\left\{1 + \left(-\frac{1247}{336} - \frac{35\eta}{12}\right)x + 4\pi x^{3/2}\right.$$
$$+ \left[\frac{6643739519}{69854400} + \frac{16\pi^2}{3} - \frac{1712\gamma_E}{105} - \frac{856}{105}\ln(16x)\right.$$
$$\left. + \left(-\frac{134543}{7776} + \frac{41\pi^2}{48}\right)\eta - \frac{94403\eta^2}{3024} - \frac{775\eta^3}{324}\right]x^3$$
$$+ \left(-\frac{16285}{504} + \frac{214745\eta}{1728} + \frac{193385\eta^2}{3024}\right)\pi x^{7/2}$$
$$+ \left(-\frac{44711}{9072} + \frac{9271\eta}{504} + \frac{65\eta^2}{18}\right)x^2$$
$$+ \left(-\frac{8191}{672} - \frac{583\eta}{24}\right)\pi x^{5/2}\right\}, \qquad (34)$$

with $\gamma_E \approx 0.5772$ being the Euler-Mascheroni constant. The amplitude of dominant ($l = 2$, $m = 2$) gravitational waveform mode, derived from spin-weighted spherical harmonics, is [118–120]

$$h_{22} = -8\sqrt{\frac{\pi}{5}}\frac{M_{tot}\eta}{D}e^{-2i\phi}x\left\{1 + \left(-\frac{107}{42} + \frac{55\eta}{42}\right)x\right.$$
$$+ \left[\frac{27027409}{646800} - \frac{856\gamma_E}{105} + \frac{2\pi^2}{3} + \frac{428i\pi}{105} - \frac{428}{105}\ln(16x)\right.$$
$$\left. + \left(\frac{41\pi^2}{96} - \frac{278185}{33264}\right)\eta - \frac{20261\eta^2}{2772} + \frac{114635\eta^3}{99792}\right]x^3$$
$$+ \left(-\frac{2173}{1512} - \frac{1069\eta}{216} + \frac{2047\eta^2}{1512}\right)x^2 + 2\pi x^{3/2}$$
$$+ \left[-\frac{107\pi}{21} + \left(\frac{34\pi}{21} - 24i\right)\eta\right]x^{5/2}\right\}, \qquad (35)$$

with D marking the observer-source distance, assumed as 100 Mpc in our analyses. The evolution of the binary's orbital phase Φ follows the differential equation as

$$\frac{dx}{dt} = -\frac{\mathcal{L}}{dE/dx}, \qquad (36)$$

$$\frac{d\Phi}{dt} = \frac{x^{3/2}}{M}, \qquad (37)$$

with the TaylorT4 method utilized for deriving the solutions. It is crucial to acknowledge the tidal-related effect, which, although emerging prominently at the fifth PN order, underscore a substantial role during binary inspiral phases. Hence, it is imperative to encapsulate this impact in the formulas, as given by [121–123]

$$\frac{dx}{dt} = \frac{64\eta}{5M_{tot}}x^5\{F_{3.5}^{T4}(x) + F_{Tidal}^{T4}(x)\}, \qquad (38)$$

where $F_{3.5}^{T4}(x)$ under the TaylorT4 approach gives as

$$F_{3.5}^{T4}(x) = 1 - \left(\frac{743}{336} + \frac{11}{4}\eta\right)x + 4\pi x^{3/2} + \left(\frac{34103}{18144}\right.$$
$$\left. + \frac{13661}{2016}\eta + \frac{59}{18}\eta^2\right)x^2 - \left(\frac{4159}{672} + \frac{189}{8}\eta\right)\pi x^{5/2}$$
$$+ \left[\frac{16447322263}{139708800} - \frac{1712}{105}\gamma_E - \frac{56198689}{217728}\eta\right.$$
$$+ \frac{541}{896}\eta^2 - \frac{5605}{2592}\eta^3 + \frac{\pi^2}{48}(256 + 451\eta)$$
$$\left. - \frac{856}{105}\ln(16x)\right]x^3 + \left(-\frac{4415}{4032}\right.$$
$$\left. + \frac{358675}{6048}\eta + \frac{91495}{1512}\eta^2\right)\pi x^{7/2}. \qquad (39)$$

The $F_{Tidal}^{T4}(x)$ denotes the tidal-related correction term, according to Vines [98], under 1PN approximation it gives as

$$F_{\text{Tidal}}^{\text{T4}}(x) = \frac{32\chi_1\lambda_2}{5M_{\text{tot}}^6}\left[12(1+11\chi_1)x^{10} + \left(\frac{4421}{28}\right.\right.$$
$$\left.\left. -\frac{12263}{28}\chi_2 + \frac{1893}{2}\chi_2^2 - 661\chi_2^3\right)x^{11}\right] + (1 \leftrightarrow 2),$$

with $\chi_1 = M_1/M_{\text{tot}}$ and $\chi_2 = M_2/M_{\text{tot}}$ marking the mass ratios and λ_1, λ_2 their respective tidal deformability. For equal-mass systems, $F_{\text{Tidal}}^{\text{T4}}(x)$ simplifies to [122]

$$F_{\text{Tidal}}^{\text{T4}}(x) = \frac{52}{5M_{\text{tot}}}\frac{k_2}{C^5}x^{10}\left(1 + \frac{5203}{4368}x\right), \qquad (40)$$

where k_2 and C describe tidal-Love number and stellar compactness parameter. This study focuses on a typical $1.35M_\odot$ equal-mass binary inspiral system, analyzing the feature of gravitational wave frequency and amplitude for quark and DM components in NSs. The integral equation is initialized with the lowest frequency as $f = 371$ Hz, correlating to $M_{\text{tot}}\Omega_0 = 0.0155$. Observers determine the source by use the retarded time defined as $t_{\text{ret}} = t - r_*$ with r_* as the tortoise coordinate, expressed by [122]

$$r_* = r_A + 2M_{\text{tot}}\ln\left(\frac{r_A}{2M_{\text{tot}}} - 1\right), \qquad (41)$$

with $r_A = \sqrt{A/4\pi}$, and A signifying the area of proper sphere surface.

Figure 6 depicts the gravitational wave frequencies as a function of retarded time during the inspiral phase of different binary systems. In the upper panel, we conduct a comparative analysis for binary hybrid stars and binary DM-mixed hybrid stars against the benchmark of binary NSs. Specifically, in contrast to the gravitational wave frequency of binary NS inspiral, marked by a black solid line at 1688.97 Hz, the hybrid star in its final inspiral stage achieves a higher gravitational wave frequency, with a value of 1870.05 Hz. The case of DM-hybrid stars further increases the gravitational wave frequency, as shown by the dark-blue dashed line and the green solid line in the figure, which correspond to frequencies of 2270.73 Hz for $m_\phi = 20$ MeV and 2278.14 Hz for $m_\phi = 15$ MeV, respectively. Moreover, the inspiral stage also exhibits distinct retarded times among these systems, with the binary NS inspiral having the shortest retarded time of 0.06531s, followed by binary hybrid stars at 0.06567s, and the longest being for binary DM-mixed hybrid stars at 0.0666s and 0.06677s. Similar conclusions are drawn for the inspiral process of strange quark stars and DM-mixed strange quark stars, as shown in the lower panel, exhibiting higher gravitational wave frequencies and longer retarded times compared to traditional NSs, with detailed numerical results also listed in Table II. It is noteworthy that the impact of mediator mass m_ϕ in the inspiral stage is minimal, a reason that can be inferred from Figs. 4 and 5. This is because at
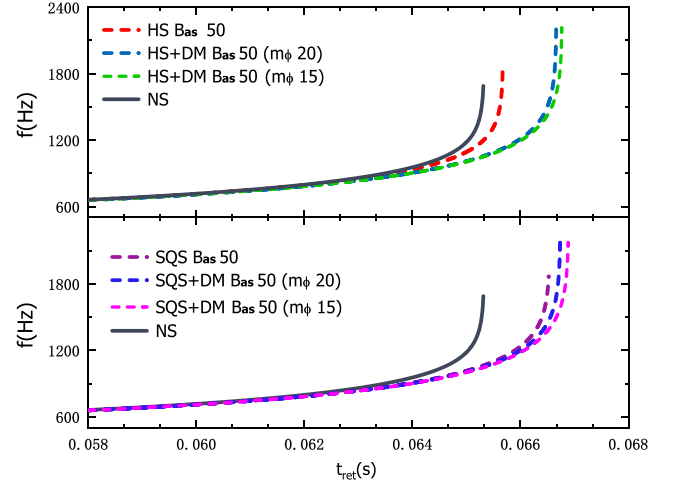
FIG. 6. Upper panel: gravitational wave frequency f during inspiral phase as a function of retarded time t_{ret} for $1.35M_\odot$ equal-mass binary compact star system. The curves represent different scenarios: binary NSs (black line), binary hybrid stars (red dashed line), binary DM-mixed hybrid stars with $m_\phi = 20$ MeV (dark-blue dashed line) and $m_\phi = 15$ MeV (green dashed line). Lower panel: gravitational wave frequency f as a function of retarded time t_{ret} for binary NSs (black line), binary strange quark stars (dark-purple dashed line), binary DM-mixed strange quark stars with $m_\phi = 20$ MeV (blue dashed line) and $m_\phi = 15$ MeV (pink dashed line).

$1.35M_\odot$, the tidal deformability values given by DM-mixed stars under different mediator masses are very close, naturally resulting in a minimal impact of tidal-related corrections on inspiral stage. Furthermore, Fig. 7 presents the gravitational wave orbital phases under the PN approximation, revealing near-identical orbital phases provided by different models over time.

Figure 8 presents the gravitational wave strain amplitude of the (2, 2) dominant mode, h_{22}, as a function of retarded time during the inspiral stage of a typical equal-mass binary star system with $1.35M_\odot$ components. The waveform of traditional binary NSs, composed purely of nucleons, is represented by the black solid line. The subfigures illustrate

TABLE II. The frequencies and retarded times in binary star inspiral phase for traditional NS, HS, HS + DM, SQS, and SQS + DM.

Case	Frequency (Hz)	t_{ret} (s)
NS	1688.97	0.06531
HS (B_{as} 50)	1870.05	0.06567
HS + DM (m_ϕ 20 B_{as} 50)	2270.73	0.06666
HS + DM (m_ϕ 15 B_{as} 50)	2278.14	0.06677
SQS (B_{as} 50)	1865.83	0.06652
SQS + DM (m_ϕ 20 B_{as} 50)	2171.17	0.06673
SQS + DM (m_ϕ 15 B_{as} 50)	2160.16	0.06689
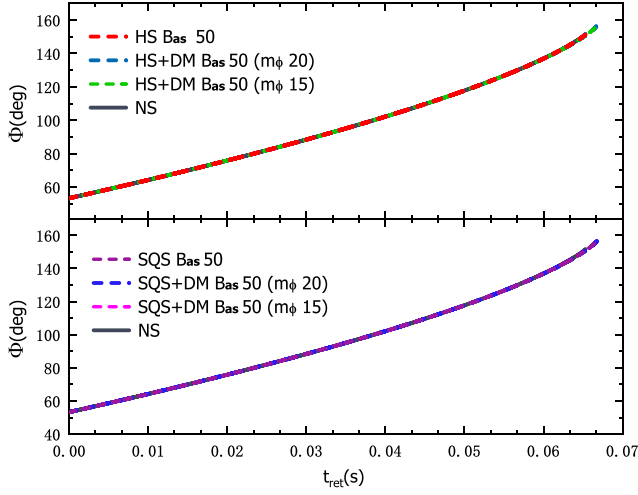
FIG. 7. Orbital phase Φ as a function of retarded time t_{ret} during inspiral phase for $1.35M_\odot$ equal-mass binary compact star system. The different color curves correspond to respective scenarios in Fig. 6.

the entire inspiral phase, where, under the PN approximation, different theoretical models all indicate a continuous increase in the gravitational wave amplitude and frequency as the inspiral phase evolves, achieving their maximal values at the final inspiral stage. Additionally, the influence of quark and DM components in various theoretical models on the waveform is not significant, primarily affecting the inspiral duration time. Specifically, in the case of binary hybrid stars system (upper panel), the inspiral stage lasts approximately 0.06567 s, slightly longer than the 0.06531 s duration for binary NSs. This suggests that the presence of quark matter prolongs the inspiral phase, meanwhile, emitting higher gravitational wave frequencies (as shown in Fig. 6). After mixing DM component, as depicted by the dark-blue and green dashed lines representing different mediator mass scenarios of $m_\phi = 20$ and 15 MeV, furthers extends the inspiral duration to 0.06666 s and 0.06677 s, respectively, introducing a delay of about 1.5 ms compared to traditional binary NSs. To analyze these results, one can
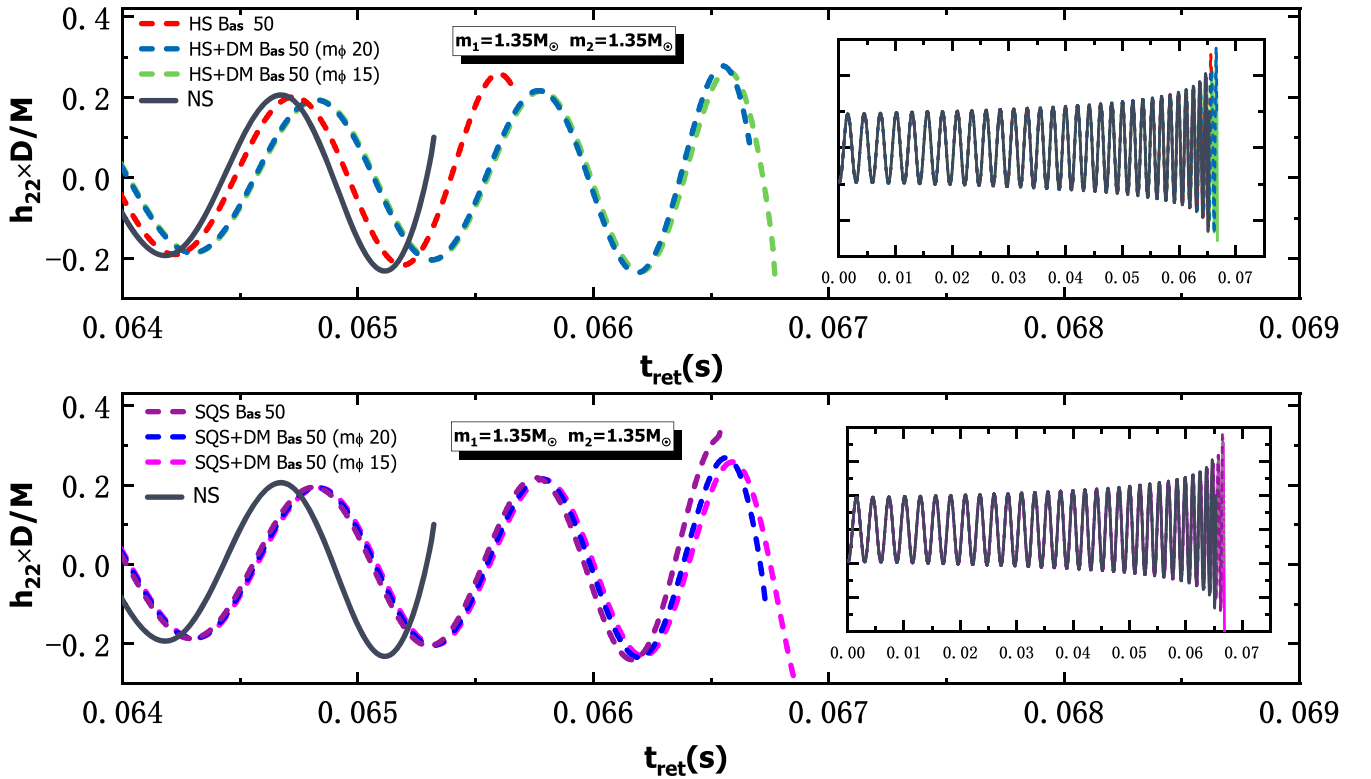
FIG. 8. Upper panel: gravitational wave amplitude h_{22} as a function of retarded time t_{ret} during inspiral phase for $1.35M_\odot$ equal-mass binary compact star system: binary NSs (black line), binary hybrid stars (red dashed line), binary DM-mixed hybrid stars with $m_\phi = 20$ MeV (dark-blue dashed line), and $m_\phi = 15$ MeV (green dashed line). Lower panel: gravitational wave amplitude h_{22} as a function of retarded time t_{ret} for binary NSs (black line), binary strange quark stars (dark-purple), binary DM-mixed strange quark stars with $m_\phi = 20$ MeV (blue) and $m_\phi = 15$ MeV (pink).

start from the perspective of mass-radius relations and tidal deformability, as the appearance of quark matter results in a smaller radius for $1.35M_\odot$ hybrid star [shown in Fig. 1(a)], making it more challenging to occur quadrupolar tidal distortion (as indicated in Figs. 4 and 5), thus diminishing the tidal-related effects during the binary inspiral stage and prolonging its duration. The DM components mixed to hybrid stars will further reduce both the radius and tidal deformability, extending the inspiral phase even more.

The lower panel addresses the case of strange quark stars. The dark-purple dash line with an inspiral duration being 0.6652 s represents the binary strange quark inspiral process. After mixing DM component, the inspiral duration of DM-mixed strange quark stars under different mediator masses are 0.06673 s and 0.06689 s, approximately 2 ms delayed compared to traditional NSs. These results share a similar behavior: the strange quark star, with smaller radius [as shown in Fig. 1(b)] and lower tidal deformability value (shown in Figs. 4 and 5), is less prone to tidal distortion, thus extending the inspiral duration.

Nevertheless, the results from Figs. 6 and 8 highlight the significant roles of quark and DM components in modulating the gravitational wave frequency and the duration of the inspiral phase. With advancements in the sensitivity of forthcoming gravitational wave detectors, like the ground-based Einstein Telescope and Cosmic Explore [124–127], as well as the space-based LISA [128], we anticipate more inspiral stage gravitational waves will be precisely captured. These results, combined with mass-radius relationship and tidal deformability analyses, will further aid in our search for signals of quark matter and DM within NSs, in turn, will also refine our understanding and constraints on theoretical models.

IV. SUMMARY

The detection of gravitational wave event GW170817 and its electromagnetic counterparts has markedly enhanced our understanding of NS internal physics, and in particular the extracted tidal deformability values offer unique advantages in constraining the nuclear EoSs. Nevertheless, such event remains scarce. Recent evidence suggests that quark matter may exist within NSs, and their strong gravitational fields could also potentially capture DMs. Searching for quark and DM signals through inspiral stage gravitational waves is an interesting idea and also one that can be tested in future gravitational wave detectors. In our study, we focus on $1.35M_\odot$ equal-mass binary inspiral process under PN approximation for hybrid stars and strange quark stars, as well as their DM-mixed counterparts. We construct traditional NSs using RMFT framework, and further construct hybrid stars and strange quark stars using a density-dependent bag model. For DM candidates, we use fermion particles to build their corresponding DM-mixed counterparts. Adjustments to the bag constant and mediator mass within these models allow us to examine the impacts of quarks and DMs. Our study finds that mixing DM components significantly soften the EoSs, especially the cases for hybrid stars, offering a potential explanation for the peculiar compact object in the supernova remnant HESS J1731-347. Compared to traditional NSs, hybrid stars and strange quark stars, along with their DM-mixed counterparts, are less likely to undergo tidal distortion in the tidal field, thus showing minor tidal-related corrections to gravitational wave radiation during the inspiral process. Notably, hybrid stars and strange quark stars exhibit higher gravitational wave frequencies and longer inspiral durations than that of traditional NSs, with mixed-DM hybrid stars and strange quark stars further increase the frequency and inspiral time.

From the results of this study, it is clear that the effects from quark and DM can indeed play an important role in modulating gravitational wave of binary inspiral process. The detection of these effects, although still difficult, underscores the fact that inspiral gravitational waves can be used as a tool to probe the matter inside a NS. Furthermore, addressing quark and DM components in NSs can further help us to understand the EoSs under extreme conditions. Currently, the gravitational wave detectors is undergoing a significant leap, from LIGO/ Virgo-KAGRA collaboration [124,129] to future upgraded versions of Advanced LIGO Plus (A+) [129] and to next-generation detectors like the Einstein Telescope [124–126], Cosmic Explorer [127], and LISA [128]. These devices, renowned for their high sensitivity, are poised to accurately capture gravitational wave signals, and in turn help us to better check the conclusions given by theoretical hypotheses.

ACKNOWLEDGMENTS

[1] J. M. Lattimer and M. Prakash, Science **304**, 536 (2004).

[2] G. Burgio, H.-J. Schulze, I. Vidaña, and J.-B. Wei, Prog. Part. Nucl. Phys. **120**, 103879 (2021).

[3] M. Oertel, M. Hempel, T. Klähn, and S. Typel, Rev. Mod. Phys. **89**, 015007 (2017).

[4] P. B. Demorest, T. Pennucci, S. M. Ransom, M. S. E. Roberts, and J. W. T. Hessels, Nature (London) **467**, 1081 (2010).

[5] E. Fonseca, H. T. Cromartie, and T. T. Pennucci, Astrophys. J. Lett. **915**, L12 (2021).

[6] J. Antoniadis, P. C. C. Freire, N. Wex *et al.*, Science **340**, 448 (2013).

[7] B. P. Abbott, R. Abbott, T. D. Abbott *et al.* (LIGO Scientific and Virgo Collaborations), Phys. Rev. Lett. **119**, 161101 (2017).

[8] R. Abbott, T. D. Abbott, S. Abraham *et al.*, Astrophys. J. **896**, L44 (2020).

[9] M. C. Miller, F. K. Lamb, A. J. Dittmann, S. Bogdanov, Z. Arzoumanian *et al.*, Astrophys. J. **887**, L24 (2019).

[10] T. E. Riley, A. L. Watts, S. Bogdanov, P. S. Ray, R. M. Ludlam *et al.*, Astrophys. J. **887**, L21 (2019).

[11] M. C. Miller, F. K. Lamb, A. J. Dittmann, S. Bogdanov, and Z. Arzoumanian, Astrophys. J. Lett. **918**, L28 (2021).

[12] T. E. Riley *et al.*, Astrophys. J. Lett. **918**, L27 (2021).

[13] R. W. Romani, D. Kandel, A. V. Filippenko, T. G. Brink, and W. Zheng, Astrophys. J. Lett. **934**, L17 (2022).

[14] V. Doroshenko, V. Suleimanov, G. Pühlhofer, and A. Santangelo, Nat. Astron. **6**, 1444 (2022).

[15] K. Gendreau, Z. Arzoumanian, E. Ferrara, and C. B. Markwardt, *Handbook of X-ray and Gamma-ray Astrophysics* (Springer Nature, Singapore, 2022).

[16] F. J. Fattoyev, C. J. Horowitz, J. Piekarewicz, and B. Reed, Phys. Rev. C **102**, 065805 (2020).

[17] A. Sedrakian, F. Weber, and J. J. Li, Phys. Rev. D **102**, 041301 (2020).

[18] I. Bombaci, A. Drago, D. Logoteta, G. Pagliara, and I. Vidaña, Phys. Rev. Lett. **126**, 162702 (2021).

[19] S. Kubis, W. Wójcik, D. A. Castillo, and N. Zabari, Phys. Rev. C **108**, 045803 (2023).

[20] L. Brodie and A. Haber, Phys. Rev. C **108**, 025806 (2023).

[21] J. J. Li and A. Sedrakian, Phys. Lett. B **844**, 138062 (2023).

[22] B. Hong and Z. Ren, Phys. Rev. D **109**, 023002 (2024).

[23] S. Weissenborn, D. Chatterjee, and J. Schaffner-Bielich, Nucl. Phys. **A881**, 62 (2012).

[24] D. Chatterjee and I. Vidaña, Eur. Phys. J. A **52**, 29 (2016).

[25] F. Ma, W. Guo, and C. Wu, Phys. Rev. C **105**, 015807 (2022).

[26] V. B. Thapa and M. Sinha, Phys. Rev. D **102**, 123007 (2020).

[27] G. Baym, Phys. Rev. Lett. **30**, 1340 (1973).

[28] E. Farhi and R. L. Jaffe, Phys. Rev. D **30**, 2379 (1984).

[29] P. Haensel, J. L. Zdunik, and R. Schaefer, Astron. Astrophys. **160**, 121 (1986), https://ui.adsabs.harvard.edu/abs/1986A%26A...160..121H/abstract.

[30] M. Alford, D. Blaschke, A. Drago, T. Klähn, G. Pagliara, and J. Schaffner-Bielich, Nature (London) **445**, E7 (2007).

[31] M. G. Alford, S. Han, and K. Schwenzer, J. Phys. G **46**, 114001 (2019).

[32] O. Ivanytskyi and D. Blaschke, Phys. Rev. D **105**, 114042 (2022).

[33] E. Annala, T. Gorda, J. Hirvonen, O. Komoltsev, A. Kurkela, J. Nättilä, and A. Vuorinen, Nat. Commun. **14**, 8451 (2023).

[34] J. Bramante and N. Raj, Phys. Rep. **1052**, 1 (2024).

[35] A. R. Bodmer, Phys. Rev. D **4**, 1601 (1971).

[36] E. Witten, Phys. Rev. D **30**, 272 (1984).

[37] Hidezumi Terazawa, Keiichi Akama, and Yūichi Chikashige, Prog. Theor. Phys. **60**, 1521 (1978).

[38] E. Annala, T. Gorda, A. Kurkela, J. Nättilä, and A. Vuorinen, Nat. Phys. **16**, 907 (2020).

[39] M. Ferreira, R. C. Pereira, and C. M. C. Providência, Phys. Rev. D **102**, 083030 (2020).

[40] Y. Yamamoto, N. Yasutake, and T. A. Rijken, Phys. Rev. C **105**, 015804 (2022).

[41] H. Sun and D. Wen, Phys. Rev. C **108**, 025801 (2023).

[42] W.-L. Yuan, A. Li, Z. Miao, B. Zuo, and Z. Bai, Phys. Rev. D **105**, 123004 (2022).

[43] Y. Yamamoto, N. Yasutake, and T. A. Rijken, Phys. Rev. C **108**, 035811 (2023).

[44] A. Quddus, G. Panotopoulos, B. Kumar, S. Ahmad, and S. K. Patra, J. Phys. G **47**, 095202 (2020).

[45] O. Lourenço, T. Frederico, and M. Dutra, Phys. Rev. D **105**, 023008 (2022).

[46] H. C. Das, A. Kumar, B. Kumar, S. K. Biswal, T. Nakatsukasa, A. Li, and S. K. Patra, Mon. Not. R. Astron. Soc. **495**, 4893 (2020).

[47] P. Routaray, H. C. Das, S. Sen, B. Kumar, G. Panotopoulos, and T. Zhao, Phys. Rev. D **107**, 103039 (2023).

[48] A. Tan *et al.* (PandaX-II Collaboration), Phys. Rev. Lett. **117**, 121303 (2016).

[49] G. Bertone and D. Hooper, Rev. Mod. Phys. **90**, 045002 (2018).

[50] M. A. Buen-Abad, R. Essig, D. McKeen, and Y.-M. Zhong, Phys. Rep. **961**, 1 (2022).

[51] N. K. Glendenning, Phys. Lett. **114B**, 392 (1982).

[52] H. Shen, H. Toki, K. Oyamatsu, and K. Sumiyoshi, Nucl. Phys. **A637**, 435 (1998).

[53] P. Ring, Prog. Part. Nucl. Phys. **37**, 193 (1996).

[54] I. Bednarek and R. Manka, Int. J. Mod. Phys. D **10**, 607 (2001).

[55] F. J. Fattoyev, C. J. Horowitz, J. Piekarewicz, and G. Shen, Phys. Rev. C **82**, 055803 (2010).

[56] V. Parmar, H. C. Das, M. K. Sharma, and S. K. Patra, Phys. Rev. D **107**, 043022 (2023).

[57] S. Yang and D. Wen, Phys. Rev. D **107**, 063009 (2023).

[58] G. Burgio, M. Baldo, P. Sahu, A. B. Santra, and H.-J. Schulze, Phys. Lett. B **526**, 19 (2002).

[59] G. F. Burgio, M. Baldo, P. K. Sahu, and H.-J. Schulze, Phys. Rev. C **66**, 025802 (2002).

[60] C. Kouvaris and N. G. Nielsen, Phys. Rev. D **92**, 063526 (2015).

[61] B. G. Todd-Rutel and J. Piekarewicz, Phys. Rev. Lett. **95**, 122501 (2005).

[62] G. A. Lalazissis, J. König, and P. Ring, Phys. Rev. C **55**, 540 (1997).

[63] B. Kumar, S. K. Patra, and B. K. Agrawal, Phys. Rev. C **97**, 045806 (2018).

[64] W.-C. Chen and J. Piekarewicz, Phys. Lett. B **748**, 284 (2015).
[65] V. Thakur, R. Kumar, P. Kumar, V. Kumar, B. K. Agrawal, and S. K. Dhiman, Phys. Rev. C **106**, 025803 (2022).
[66] T. Miyatsu, M.-K. Cheoun, K. Kim, and K. Saito, Phys. Lett. B **843**, 138013 (2023).
[67] N. Hornick, L. Tolos, A. Zacchi, J.-E. Christian, and J. Schaffner-Bielich, Phys. Rev. C **98**, 065804 (2018).
[68] W.-C. Chen and J. Piekarewicz, Phys. Rev. C **90**, 044305 (2014).
[69] B. Hong and X.-L. Mu, Commun. Theor. Phys. **74**, 065301 (2022).
[70] C. J. Horowitz, J. Piekarewicz, and B. Reed, Phys. Rev. C **102**, 044321 (2020).
[71] E. Khan, J. Margueron, and I. Vidaña, Phys. Rev. Lett. **109**, 092501 (2012).
[72] P.-G. Reinhard, X. Roca-Maza, and W. Nazarewicz, Phys. Rev. Lett. **127**, 232501 (2021).
[73] G. Baym, C. Pethick, and P. Sutherland, Astrophys. J. **170**, 299 (1971).
[74] C. Gonzalez-Boquera, M. Centelles, X. Viñas, and L. M. Robledo, Phys. Lett. B **779**, 195 (2018).
[75] J. Carriere, C. J. Horowitz, and J. Piekarewicz, Astrophys. J. **593**, 463 (2003).
[76] D. Sen, N. Alam, and G. Chaudhuri, J. Phys. G **48**, 105201 (2021).
[77] D. Logoteta and I. Bombaci, Phys. Rev. D **88**, 063001 (2013).
[78] A. Bhattacharyya, I. N. Mishustin, and W. Greiner, J. Phys. G **37**, 025201 (2010).
[79] C. Constantinou, T. Zhao, S. Han, and M. Prakash, Phys. Rev. D **107**, 074013 (2023).
[80] M. Pospelov and A. Ritz, Phys. Rev. D **84**, 113001 (2011).
[81] B. Bhattacherjee, S. Matsumoto, S. Mukhopadhyay, and M. M. Nojiri, J. High Energy Phys. 10 (2013) 032.
[82] A. Maselli, P. Pnigouras, N. G. Nielsen, C. Kouvaris, and K. D. Kokkotas, Phys. Rev. D **96**, 023005 (2017).
[83] S. L. Shapiro and S. A. Teukolsky, *Black Holes, White Dwarfs, and Neutron Stars: The Physics of Compact Objects* (John Wiley & Sons, New York, 1983).
[84] Q.-F. Xiang, W.-Z. Jiang, D.-R. Zhang, and R.-Y. Yang, Phys. Rev. C **89**, 025803 (2014).
[85] O. Ivanytskyi, V. Sagun, and I. Lopes, Phys. Rev. D **102**, 063028 (2020).
[86] B. Kain, Phys. Rev. D **102**, 023001 (2020).
[87] M. F. Barbat, J. Schaffner-Bielich, and L. Tolos, arXiv:2404.12875.
[88] M. Hippert, E. Dillingham, H. Tan, D. Curtin, J. Noronha-Hostler, and N. Yunes, Phys. Rev. D **107**, 115028 (2023).
[89] J. E. Horvath, L. S. Rocha, L. M. de Sá, P. H. R. S. Moraes, L. G. Barão, M. G. B. de Avellar, A. Bernardo, and R. R. A. Bachega, Astron. Astrophys. **672**, L11 (2023).
[90] J. E. Nyhan and B. Kain, Phys. Rev. D **105**, 123016 (2022).
[91] R. F. Diedrichs, N. Becker, C. Jockel, J.-E. Christian, L. Sagunski, and J. Schaffner-Bielich, Phys. Rev. D **108**, 064009 (2023).
[92] J. C. Jiménez and E. S. Fraga, Universe **8** (2022).
[93] Y. Dengler, J. Schaffner-Bielich, and L. Tolos, Phys. Rev. D **105**, 043013 (2022).

[94] T. Hinderer, Astrophys. J. **677**, 1216 (2008).
[95] T. Hinderer, B. D. Lackey, R. N. Lang, and J. S. Read, Phys. Rev. D **81**, 123016 (2010).
[96] T. Malik, N. Alam, M. Fortin, C. Providência, B. K. Agrawal, T. K. Jha, B. Kumar, and S. K. Patra, Phys. Rev. C **98**, 035804 (2018).
[97] E. E. Flanagan and T. Hinderer, Phys. Rev. D **77**, 021502 (2008).
[98] J. Vines, E. E. Flanagan, and T. Hinderer, Phys. Rev. D **83**, 084051 (2011).
[99] S. Postnikov, M. Prakash, and J. M. Lattimer, Phys. Rev. D **82**, 024016 (2010).
[100] J. Hu, S. Bao, Y. Zhang, K. Nakazato, K. Sumiyoshi, and H. Shen, Prog. Theor. Exp. Phys. **2020** (2020).
[101] X. Wang, A. Kuerban, J.-J. Geng, F. Xu, X.-L. Zhang, B.-J. Zuo, W.-L. Yuan, and Y.-F. Huang, Phys. Rev. D **104**, 123028 (2021).
[102] B.-L. Li, Y. Yan, and J.-L. Ping, Phys. Rev. D **104**, 043002 (2021).
[103] E.-P. Zhou, X. Zhou, and A. Li, Phys. Rev. D **97**, 083015 (2018).
[104] M. B. Albino, R. Fariello, and F. S. Navarra, Phys. Rev. D **104**, 083011 (2021).
[105] A. Das, T. Malik, and A. C. Nayak, Phys. Rev. D **105**, 123034 (2022).
[106] E. Burns, Living Rev. Relativity **23**, 4 (2020).
[107] J. A. Faber and F. A. Rasio, Living Rev. Relativity **15**, 8 (2012).
[108] D. Radice, S. Bernuzzi, and A. Perego, Annu. Rev. Nucl. Part. Sci. **70**, 95 (2020).
[109] L. Blanchet, Living Rev. Relativity **9**, 4 (2006).
[110] M. Boyle, D. A. Brown, L. E. Kidder, A. H. Mroué, H. P. Pfeiffer, M. A. Scheel, G. B. Cook, and S. A. Teukolsky, Phys. Rev. D **76**, 124038 (2007).
[111] H. C. Das, A. Kumar, and S. K. Patra, Mon. Not. R. Astron. Soc. **507**, 4053 (2021).
[112] A. Buonanno and B. S. Sathyaprakash, arXiv:1410.7832.
[113] L. Blanchet, G. Faye, and F. Larrouturou, Classical Quantum Gravity **39**, 195003 (2022).
[114] A. Chattaraj, T. RoyChowdhury, Divyajyoti, C. K. Mishra, and A. Gupta, Phys. Rev. D **106**, 124008 (2022).
[115] B. D. Lackey, The neutron-star equation of state and gravitational waves from compact binaries, Ph.D. thesis, The University of Wisconsin-Milwaukee, 2012.
[116] M. Maggiore, *Gravitational Waves: Volume 1: Theory and Experiments* (Oxford University Press, New York, 2007).
[117] L. Blanchet, B. R. Iyer, and B. Joguet, Phys. Rev. D **65**, 064005 (2002).
[118] L. E. Kidder, Phys. Rev. D **77**, 044016 (2008).
[119] Q. Henry, Phys. Rev. D **107**, 044057 (2023).
[120] G. Faye, S. Marsat, L. Blanchet, and B. R. Iyer, Classical Quantum Gravity **29**, 175004 (2012).
[121] A. Buonanno, B. R. Iyer, E. Ochsner, Y. Pan, and B. S. Sathyaprakash, Phys. Rev. D **80**, 084043 (2009).
[122] K. Hotokezaka, K. Kyutoku, and M. Shibata, Phys. Rev. D **87**, 044001 (2013).
[123] K. Hotokezaka, K. Kyutoku, Y.-i. Sekiguchi, and M. Shibata, Phys. Rev. D **93**, 064082 (2016).
[124] S. E. Perkins, N. Yunes, and E. Berti, Phys. Rev. D **103**, 044024 (2021).

[125] M. Punturo, M. Abernathy, F. Acernese *et al.*, Classical Quantum Gravity **27**, 084007 (2010).

[126] S. Dwyer, D. Sigg, S. W. Ballmer, L. Barsotti, N. Mavalvala, and M. Evans, Phys. Rev. D **91**, 082001 (2015).

[127] M. Evans, R. X. Adhikari, C. Afle *et al.*, arXiv:2109.09882.

[128] P. Amaro-Seoane, H. Audley, S. Babak, J. Baker, E. Barausse, P. Bender, E. Berti, P. Binetruy, M. Born, and D. Bortoluzzi, arXiv:1702.00786.

[129] B. P. Abbott, R. Abbott, T. D. Abbott, S. Abraham *et al.*, Living Rev. Relativity **23**, 3 (2020).